J. Fluid Mech. (2011), *vol.* 680, *pp.* 477–487.
doi:10.1017/jfm.2011.210

Liquid spreading on superhydrophilic micropillar arrays

SEONG JIN KIM[1], MYOUNG-WOON MOON[2], KWANG-RYEOL LEE[2], DAE-YOUNG LEE[2], YOUNG SOO CHANG[3] AND HO-YOUNG KIM[1]†

[1]School of Mechanical and Aerospace Engineering, Seoul National University, Seoul 151-744, Korea

[2]Korea Institute of Science and Technology, Seoul 136-791, Korea

[3]Department of Advanced Fermentation Fusion Science and Technology, Kookmin University, Seoul 136-702, Korea

(Received 29 July 2010; revised 21 April 2011; accepted 9 May 2011; first published online 20 June 2011)

When a drop is deposited on a superhydrophilic micropillar array, the upper part of the drop (referred to as the bulk) collapses while the bottom part penetrates into the gaps of the array, forming a fringe film. Here we quantify the early stage dynamics of this process using a combination of experiment and theory. We show that the circular front of the fringe film spreads like $t^{1/2}$, t being time, when coupled to the bulk flow. However, the film is found to advance like $t^{1/3}$ through faceted zippering in the absence of the bulk. We then show that the spreading of the bulk and the entire drop footprint follows a power law ($t^{1/4}$) that is different from Washburn's law. This work can be a starting point to completely understand the spreading of liquids on superhydrophilic surfaces and opens questions specific to superwetting behaviour including the criteria to determine whether the fringe film will expand through lateral zipping or advance radially outwards.

Key words: capillary flows, microfluidics, thin films

1. Introduction

The spreading behaviour of a liquid drop on a highly wettable smooth solid surface has been the subject of intense study for decades. By considering the forces exerted on the drop including surface tension, gravity and viscous forces, several power laws have been proposed to predict the degree of drop spreading with time. Tanner (1979) first considered the spreading of a small liquid drop driven by surface tension and resisted by viscosity to propose a power law of the spreading radius, $R \sim t^{1/10}$, where t is time. For the late stage of spreading of a large drop mainly driven by gravity, the radius increases with $t^{1/8}$ and with $t^{1/7}$ when the dissipation occurs in the bulk (Lopez & Miller 1976; Huppert 1982) and near the contact line (Ehrhard 1993), respectively. Biance, Clanet & Quéré (2004) showed that the inertia resists the capillary driven spreading in the very early stages, leading to $R \sim t^{1/2}$.

When a solid surface is micropatterned, its intrinsic wettability is magnified so that the hydrophilic surface becomes superhydrophilic. Even a superhydrophobic surface can act as a superwetting surface for low-surface-tension liquids, such as oils

† Email address for correspondence: hyk@snu.ac.kr

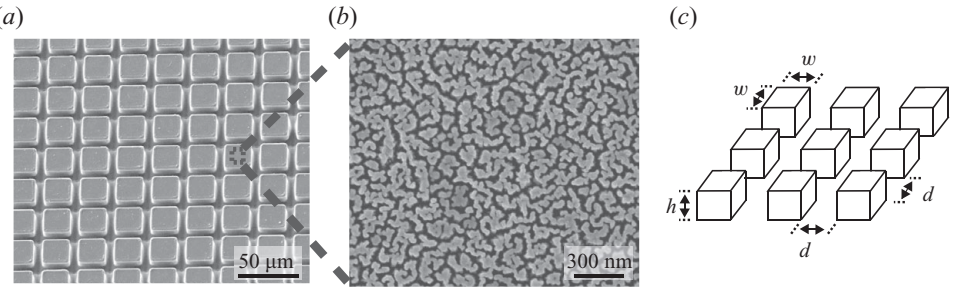

FIGURE 1. (*a*) A scanning electron microscopy image of the square micropillar array covered with (*b*) nanoscale roughness. (*c*) Schematic of the square micropillar array.

(McHale *et al.* 2004). Two important distinct features of the spreading behaviour on the micropillar arrays were previously identified – the drop may spread into polygonal, not circular, films depending on the wettability of the original smooth surface and the geometry of the micropatterns, and the spreading edge propagates through a zipping mechanism in the late stages of spreading so that the wet area expands by filling the rows of pillars along the edge (Courbin *et al.* 2007). Such features were also observed for the drop wetting into the micropillars of a superhydrophobic surface (Sbragaglia *et al.* 2007) as air pockets supporting the drop collapse, corresponding to the transition from the Cassie state (Cassie & Baxter 1944) to the Wenzel state (Wenzel 1936). Wicking of a liquid film into vertically situated wettable micropillar arrays against gravity was studied by Ishino *et al.* (2007). Reyssat *et al.* (2008) showed that the geometric variations of the solid surface can modify the classical equation of Washburn (1921) for the spreading rate.

When a drop is brought into contact with a superhydrophilic micropillar array, the upper part of the drop, referred to as the bulk, collapses, while the bottom part penetrates into the gaps of the array. The bulk vanishes towards the end of the spreading process when the film extension dominates the flow. Although Courbin *et al.* considered the spreading rate of a thin fringe film around the collapsing drop in the late stages, it has not been investigated how the drop spreads in the early stages, which we aim to address in this work. Since the mechanisms that induce the drop collapse and the fringe propagation are qualitatively different, separate considerations should be given for the macroscopic bulk flow and the microscopic film extension. When coupled to the bulk flow, the circular front of the fringe film spreads initially, but the film is found to advance through faceted zippering in the absence of the bulk. We compare the film propagation rates of the two different modes, although the criteria to determine whether the fringe film will expand through lateral zipping or advance radially outwards are still unclear. In the following, we first describe the experiments to observe the spreading of liquids on superhydrophilic micropillar arrays. Then theoretical models – power laws – are constructed to elucidate the physics underlying the spreading phenomena and experimentally corroborated.

2. Experiments

To fabricate micropillar arrays on an Si wafer, we etch the Si(1 0 0) surface using the deep reactive ion etching process. Figure 1 shows the images of a resulting surface. We vary the height (h), width (w) and spacing (d) of the square pillars as shown in figure 1(c) to investigate the effects of the microtextures on the spreading dynamics, so

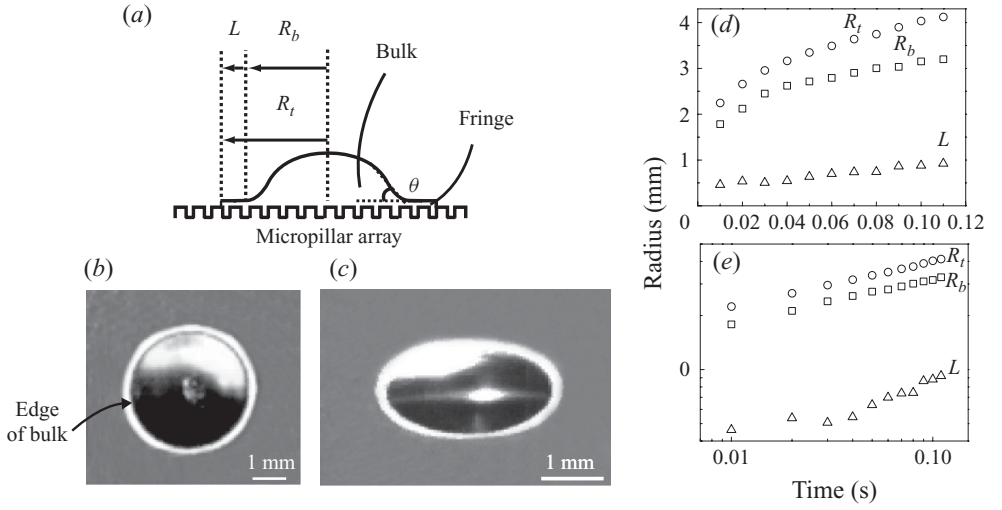

FIGURE 2. (*a*) Schematic of a liquid drop spreading on a hydrophilic micropillar array. R_b and R_t indicate the radii of the bulk and the entire drop footprint, and the length of fringe layer $L = R_t - R_b$. (*b*) A top view and (*c*) a tilted view of a spreading silicone oil drop on the micropillar array with $[h, d, w] = [16, 15, 20]$ μm. (*d*) Linear and (*e*) log–log plot of the experimentally measured spreading extents of a water drop with $a = 0.7$ mm deposited on a micropillar array with $[h, d, w] = [10, 20, 10]$ μm versus time.

that $\{h, w, d\} \in [10\ 20]$ μm. The wafer is cleaned with Ar gas and then coated with the Si–incorporated diamond-like carbon film using the gas mixture of benzene and silane in a radio frequency–chemical vapour deposition chamber. Finally, oxygen plasma etching is carried out to create hydrophilic Si–O bonds and nanoscale roughness on the surface as shown in figure 1(*b*). For more detailed process conditions, see Yi *et al.* (2010). The result is a hierarchical superhydrophilic surface, i.e. a highly wettable surface with both micro- and nano-scopic roughness. As drop liquids, we use deionized water with density $\rho = 1000\,\mathrm{kg\,m^{-3}}$, viscosity $\mu = 1.3 \times 10^{-3}\,\mathrm{Pa\,s}$ and surface tension $\gamma = 0.074\,\mathrm{N\,m^{-1}}$ and silicone oil with $\rho = 980\,\mathrm{kg\,m^{-3}}$, $\mu = 0.091\,\mathrm{Pa\,s}$ and $\gamma = 0.021\,\mathrm{N\,m^{-1}}$. Both the liquids completely wet the micropillar arrays, thus the equilibrium contact angle of the liquids with the surfaces is nearly zero. The capillary length defined as $l_c = (\gamma/\rho g)^{1/2}$ is 2.74 and 1.48 mm for water and silicone oil, respectively. Drops of various radii, $a \in [0.5\ 1.2]$ mm, are deposited on the horizontally situated micropillar arrays using a polymeric micropipette (Rainin RC-10/10). A high-speed camera system records the liquid motion at a frame rate up to $3000\,\mathrm{s^{-1}}$.

As figure 2 shows, the drop spreading on the superhydrophilic surface consists of two distinct liquid motions – collapse of the bulk and propagation of the fringe film. Both the liquids used in this work showed the similar behaviour. The imbibition in the microscale roughness facilitates the collapse of the drop, and at the same time, the collapsing drop can push the fringe film outwards. Figures 2(*d*) and 2(*e*) show the measurement results using a water drop for the spreading radii of the bulk and the entire footprint and the difference between them corresponding to the radial extension of the fringe film.

Before analysing the spreading rates of the bulk and the fringe film, we first identify the role of the bulk by comparing the film propagation behaviours with and without the bulk. Thus we start with the film propagation in the absence of the collapsing

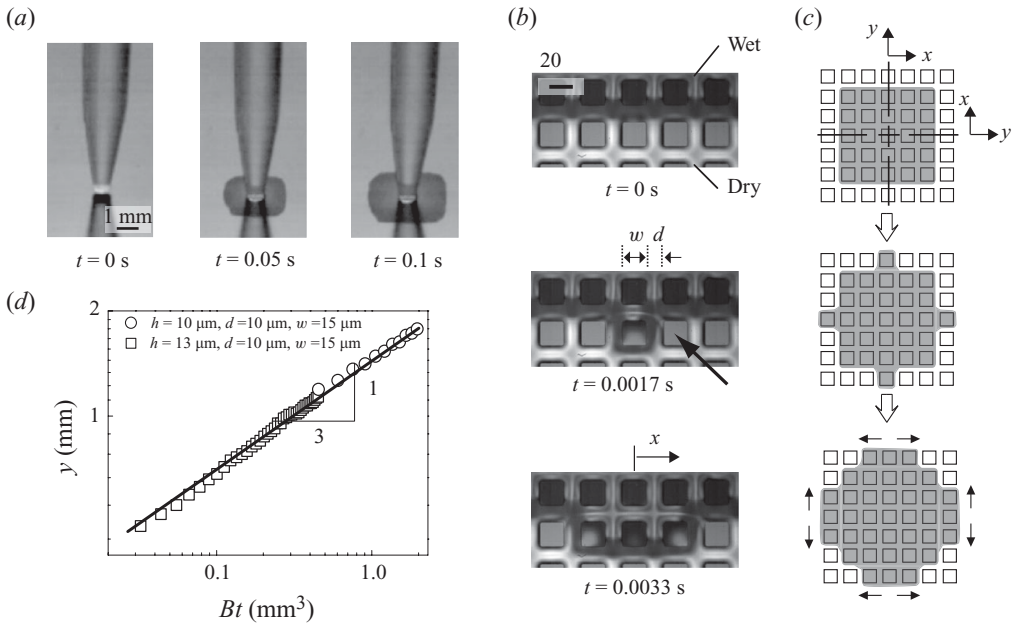

FIGURE 3. (*a*) Propagation of a film emerging from the tip of a micropipette in contact with the micropillar array. (*b*) Zipping of a protruding step along the liquid film edge. (*c*) Schematic of the wet area expansion through the zipping mechanism. On each side, x and y denotes the zipping and the expansion directions, respectively. (*d*) Edge propagation of films of water on different micropillar arrays versus time, which follows the scaling law (3.6).

bulk. To realize such film propagation, it was found to be essential to prevent the leakage of the bulk flow so that the liquid may wet only through the spacing between the pillars. To this end, we bring the tip of the polymeric pipette or a thin hypodermic needle onto the surface as shown in figures 3(*a*) and 4(*a*), respectively, and press the tip onto the substrate to induce conformal contact between them before bulk leaks from a gap either by capillarity or gravity. In what follows, we provide experimental results and theoretical considerations for this film flow first and then those for the fringe extension under the effect of the collapsing bulk. Finally we analyse the rate of the bulk collapse to explain the spreading rate of the entire footprint in the early stages.

3. Propagation of film without bulk

We consider the motion of a liquid film as pulled out from a pipette tip by capillarity as shown in figure 3(*a*). Figure 3(*b*) shows the images of the film edge that visualize the emergence and the subsequent lateral propagation, or zipping, of a protruding step. Now we consider the time it takes for the film edge to advance one row through the zipping mechanism. It is the sum of the waiting period before the pioneering step emerges out of the existing wet front and the time for the new row to be filled with liquid. Our experiments reveal that the wait times (of the order of 1 ms) are significantly shorter than the times for zipping of an entire row (of the order of 10–100 ms). For the square area consisting of $2n \times 2n$ pillars as shown in figure 3(*c*) to be wet, the zipping of rows must have occurred n times, assuming that the zipping occurs on all the four sides. Therefore, if the time taken for each row to be wet is

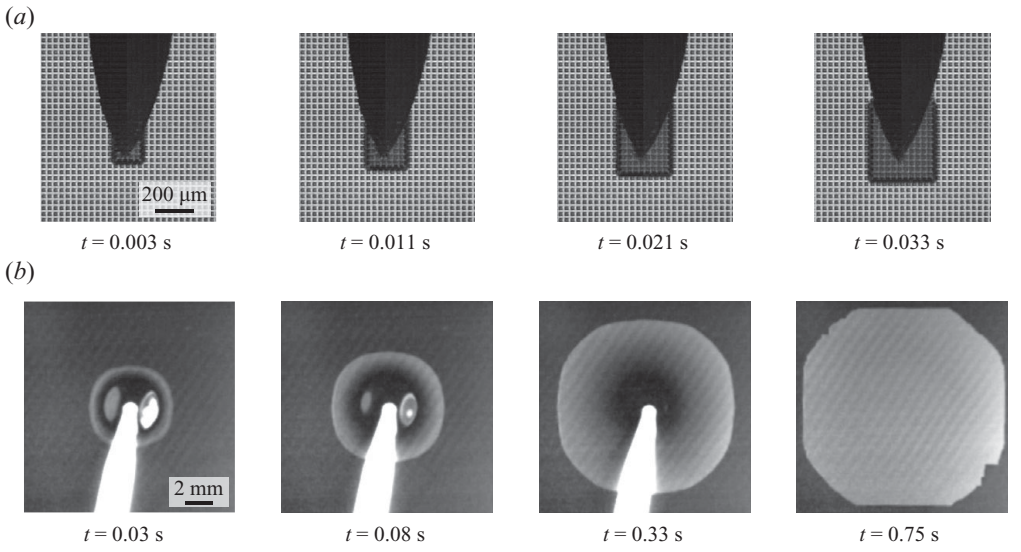

FIGURE 4. Comparison of the spreading behaviours of water films (*a*) in the absence of bulk and (*b*) driven by the bulk on the identical micropillar arrays with $h = 16\,\mu\text{m}$, $d = 15\,\mu\text{m}$ and $w = 20\,\mu\text{m}$. In (*a*), the flexible needle tip keeps its conformal contact with the substrate to result in a film flow, whereas the drop with $a = 0.7\,\text{mm}$ is separated from the pipette at $t = 0$ in (*b*).

calculated, one can easily deduce how long it takes for a given size of a square area to become wet.

Figure 3(*c*) schematically shows a liquid step zipping to the adjacent pillar. The decrease of the interfacial energy as a pillar is newly wet is given by

$$\delta E_z = \gamma(w+d)^2 + (\gamma_{SL} - \gamma_{SG})[(w+d)^2 + 4wh], \tag{3.1}$$

where γ_{SL} and γ_{SG} are the interfacial energy per unit area between solid and liquid, and solid and gas, respectively. Here we note that w and d range between 10 and 20 μm thus the front displacement associated with the wetting of a single pillar, $(w+d)$, is significantly smaller than the side length of the entire film. Thus the interfacial energy change associated with the wetting of the distance Δx in the direction of zipping can be written as $\Delta E = \Delta x \delta E_z/(w+d)$. Then we get the driving force that causes the spontaneous wicking through zipping as the following:

$$F_{d,z} = -\frac{\mathrm{d}E}{\mathrm{d}x} = (w+d)(r-1)\gamma, \tag{3.2}$$

where we have used Young's equation, $\gamma\cos\theta_e = \gamma_{SG} - \gamma_{SL}$ with the equilibrium contact angle $\theta_e \approx 0$ and r is the roughness defined as the ratio of the actual surface area to the projected area, so that $r = 1 + 4wh/(w+d)^2$. Although the top of pillars is wetted by liquid in this work, we get $F_{d,z} = \gamma(w+d)[r\cos\theta_e - 1 + \phi_t(1-\cos\theta_e)]$ with $\phi_t = w^2/(w+d)^2$ being the area fraction of the pillar top when the top remains dry and the solid is partially wettable.

Investigating the images of a zipping front, we find that a dry pillar adjacent to the curved wetting front, as designated by a thick arrow in the second image of figure 3(*b*), is wetted by a contact line from the previous row of pillars. Since the entire wet area is a thin film, the liquid that wets a new pillar and its neighbour must come from the liquid source at the centre (pipette) a distance away of $\sim y$. Therefore, the viscous

resisting force is scaled as $F_{r,z} \sim (w+d)y\sigma$, where σ is the viscous shear stress as estimated in the Appendix. For the zipping flow, $\sigma \sim (\mu r/h)(\mathrm{d}x/\mathrm{d}t)$. For the thin film flow with the Reynolds number defined as $Re = Uh/\nu$, $Re \sim 10^{-1}$ for water drops and $Re \sim 10^{-3}$ for silicone oil drops, where U is the representative film propagation speed and ν the kinematic viscosity, based on the experimental measurements; thus we neglect the flow inertia. Now balancing the driving force $F_{d,z}$ and the resisting force $F_{r,z}$ leads to the following relationship of the zipping distance x to time t:

$$x \sim \frac{\gamma h(r-1)}{\mu r y} t. \tag{3.3}$$

When an edge of the wet area covering $2(k-1) \times 2(k-1)$ pillars extends to the next row, the zipping should occur over $2k$ pillars. Here we make a simplifying assumption that a pioneering step emerges near the centre of each side and that the zipping propagates in both $+x$ and $-x$ directions, which is commonly observed in our experiments. Thus we consider the time taken for k pillars to be wet, t_k, which can be readily given by using (3.3):

$$t_k \sim \frac{\mu r k^2 (w+d)^2}{\gamma(r-1)h}, \tag{3.4}$$

where we used $x = y = k(w+d)$. Therefore, the total time, t, taken for the film to cover $2n \times 2n$ pillars is

$$t = \sum_{k=1}^{n} t_k \sim \frac{\mu r n(n+1)(2n+1)(w+d)^2}{6\gamma(r-1)h}. \tag{3.5}$$

Noting that the distance of the edge of the film from the centre of the square wet area is $y = n(w+d)$ and that $n \gg 1$, we get the relationship between the film extension y and time t as

$$y \sim (Bt)^{1/3}, \tag{3.6}$$

where $B = 3\gamma h(r-1)(w+d)/(\mu r)$. This reveals that unlike the zipping that extends with a constant velocity at a given y, the wetting front advances like $t^{1/3}$. We compare the theory with the experimental measurement of water films propagating on different pillar arrays in figure 3(*d*), to show that the power law is in good agreement with experiment. A linear regression analysis using the least square method finds the proportionality constant in (3.6) to be 1.47, i.e. $y \approx 1.47(Bt)^{1/3}$.

4. Spreading of fringe film with bulk

Figure 4 compares the spreading behaviours of water films (*a*) in the absence of bulk and (*b*) driven by the bulk on identical micropillary arrays. While the liquid wets a square area in (*a*), it spreads into a circular area in (*b*). This clearly reveals the effect of the bulk on the dynamics of film propagation. When the film spreads without the bulk, it is driven by the localized process to reduce the free energy by wetting the adjacent pillars – the free energy change associated with wetting an adjacent pillar in the same row is $\delta E_z = -4wh\gamma < 0$ with $\theta_e \approx 0$. The energy change associated with wetting a single pillar in the next row is $\delta E_a = 2h(d-w)\gamma$, which is positive for $d > w$. Even when it is negative with $d < w$, $\delta E_z < \delta E_a$, indicating that the zipping along the edge is energetically more favourable than the radial expansion. On the other hand, the circular area wetted by the fringe layer when coupled with the bulk implies that

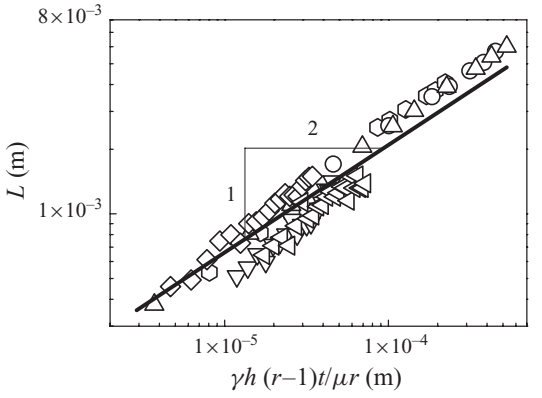

	Liquid	a (mm)	h (μm)	w (μm)	d (μm)
⬡	Oil	0.6	13	10	10
○	Oil	0.7	13	15	10
△	Oil	0.7	13	20	10
▽	Water	0.7	10	10	15
◇	Water	0.7	10	10	20
◁	Water	0.7	10	15	10

FIGURE 5. The distance between the outer edges of the bulk and the fringe, L, versus time plotted according to the scaling law (4.1).

the film flow is no longer dominated by the localized imbibition into the gaps of adjacent pillars.

Now we predict the circular spreading rate of the fringe whose radial extension $L = R_t - R_b$, where R_t and R_b are the radius of the bottom of the entire drop and the bulk, respectively. The Laplace pressure of the bulk and the fringe edge is estimated as $\sim\gamma(R_b^{-1} + H_b/R_b^2)$ and $\sim\gamma(R_t^{-1} - h^{-1})$, respectively, where H_b is the bulk height. Because $h \ll R_b$, $h \ll R_t$ and $h \ll R_b^2/H_b$, the driving capillary force, F_c, is dominantly given by the meridional curvature (h^{-1}) of the fringe edge. In a manner similar to that used to derive (3.2), we obtain F_c by considering the surface energy change associated with the increase of the fringe area, $\mathrm{d}E_c = \pi[\gamma + r(\gamma_{SL} - \gamma_{SG})]\mathrm{d}(R_t^2 - R_b^2) \approx -2\pi R_t(r-1)\mathrm{d}L$ because $L \ll R_b$ and $L \ll R_t$ in the early spreading stages as can be checked in figure 2(*d*). Then $F_c = -\mathrm{d}E_c/\mathrm{d}L = 2\pi R_t(r-1)\gamma$. The resisting force scales as $F_{r,f} \sim \pi\sigma(R_t^2 - R_b^2)$, where the shear stress σ is given in the Appendix. Balancing the driving and the resisting forces leads to

$$L \sim \left(\frac{r-1}{r}\frac{\gamma h}{\mu}\right)^{1/2} t^{1/2}, \tag{4.1}$$

where we assumed that R_b and R_t scale similarly as will be verified in the next section. The scaling law indicates that the fringe layer extends faster with the increase of the roughness, the surface tension and the pillar height, and the decrease of the viscosity. In a dimensionless form, we write $L/a \sim (t/\tau_L)^{1/2}$, where the characteristic time scale for the annular fringe layer to extend by a, $\tau_L = \mu a^2 r/[\gamma h(r-1)]$. Figure 5 shows that the experimentally measured values of L follow our scaling law. A linear regression analysis finds the proportionality constant in (4.1) to be 0.256.

Our analysis reveals that the extension of the fringes with and without the bulk is commonly caused by the capillary pressure associated with the meridional curvature of the thin film ($\sim h^{-1}$). We compare the spreading speeds of the two kinds of fringes in figure 6 together with the rate of increase of the bulk radius R_b which is given in the next section. To find the rates, we take the time derivatives of the scaling laws (3.6), (4.1) and (5.1) with the empirical proportionality constants. Figure 6(*a*) shows that $\mathrm{d}R_b/\mathrm{d}t$ is initially greater than $\mathrm{d}y/\mathrm{d}t$, which suggests that when coupled to a bulk collapse, the fringe film spreads (or is pushed by the bulk) too fast for the contact line to be pinned temporarily on rows of pillars; thus circular spreading is

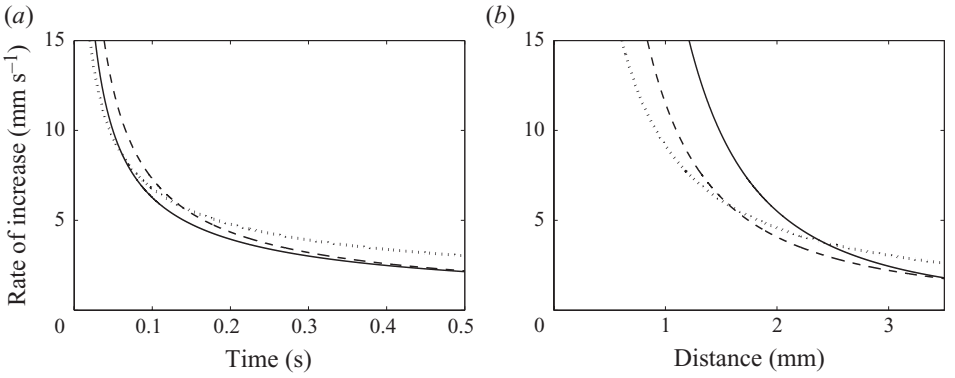

FIGURE 6. Comparison of the rates of increase, $\mathrm{d}y/\mathrm{d}t$ (solid line), $\mathrm{d}R_b/\mathrm{d}t$ (dashed line) and $\mathrm{d}L/\mathrm{d}t$ (dotted line), on the pillar array with $h = d = 10\,\mu\mathrm{m}$ and $w = 15\,\mu\mathrm{m}$. (*a*) The rates versus time measured from the first contact of the water with the substrate. (*b*) The rates versus the fringe film size: $\mathrm{d}y/\mathrm{d}t$ versus y, and $\mathrm{d}R_b/\mathrm{d}t$ and $\mathrm{d}L/\mathrm{d}t$ versus L.

observed. However, when we plot the expansion rates versus the distance that a liquid should travel from the source to the edge of the fringe (L and y for the film with and without bulk, respectively) in figure 6(*b*), it is found that $\mathrm{d}y/\mathrm{d}t$ exceeds both $\mathrm{d}R_b/\mathrm{d}t$ and $\mathrm{d}L/\mathrm{d}t$ initially. This indicates that the liquid film can extend to the next row more efficiently through the zipping mechanism than by advancing the entire contact line. It is mainly because the gap between the rows of pillars is rapidly filled with liquid at a rate $\mathrm{d}x/\mathrm{d}t$ when the lateral zipping occurs, thus the next row gets wet faster than when the circular spreading takes place. However, as the wetted area increases, the time taken to fill the gap through zipping increases, so that the expansion by such a mechanism becomes slower than the circular spreading.

5. Spreading of bulk and entire drop

Now we turn to a power law that can predict the rate of the bulk spreading that occurs on top of the underlying film as illustrated in figure 2(*a*). The continual expansion of the fringe film implies that the liquid in the bulk is drained into the film causing the volume of the bulk to decrease with time. Consequently, the radius of the bulk increases in the early stages of spreading but decreases in the late stages before it vanishes eventually. Here we aim to understand the early time behaviour of the bulk spreading.

On the prewetted surface that has been formed by liquid imbibition into the forest of micropillars, the magnitude of the driving force for the bulk spreading due to capillarity is $F_{d,b} \sim R_b\gamma(1-\cos\theta)$, where θ is the advancing contact angle (de Gennes 1985). Except for the extremely early stages where the drop is nearly spherical, $H_b \ll R_b$; thus the lubrication approximation holds. The characteristic velocity gradient in the bulk is of order $\dot{R}_b/R_b$ since there is effectively velocity slip in the bottom due to fast drainage into pillar gaps (Brochard-Wyart, Debrégeas & de Gennes 1996). Now balancing the viscous resistant force $F_{r,b} \sim \mu H_b R_b(\dot{R}_b/R_b)$ with $F_{d,b} \sim \gamma R_b\theta^2$ leads to $\dot{R}_b \sim (\gamma/\mu)(H_b/R_b)$, where we used $\theta \approx H_b/R_b$. The temporal evolution of H_b is obtained by scaling the instantaneous bulk volume as $R_b^2 H_b \sim (4/3)\pi a^3 - \pi h f(R_t^2 - R_b^2)$, where $f = 1 - w^2/(w+d)^2$ corresponds to the ratio of the basal area not covered by pillars to the entire projected area. By conservatively taking $R_t^2 - R_b^2 \sim aL$ and using (4.1), it can be shown that the volume drained to the

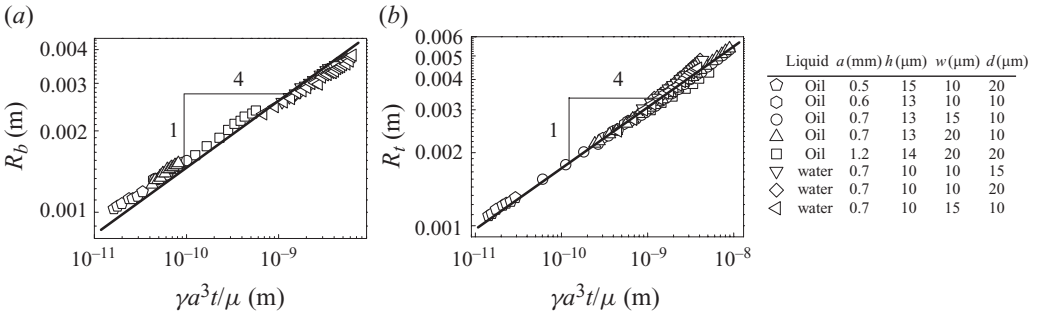

FIGURE 7. The experimentally measured (*a*) bulk radius and (*b*) entire footprint radius versus time plotted according to the scaling law (5.1) and (5.2), respectively.

fringe, $\pi hf(R_t^2 - R_b^2)$, is negligibly small compared to the original drop volume when $t \ll t_c$, where $t_c = a^4\mu r/[f^2\gamma h^3(r-1)]$. Then we write $H_b \sim (4/3)\pi a^3/R_b^2$ for $t \ll t_c$. The typical orders of t_c are 10 and 10^4 s and the measurements of R_b were performed for ~ 0.1 and 10 s for water and silicone oil drops, respectively. Then R_b is scaled as

$$R_b \sim \left(\frac{\gamma a^3}{\mu}\right)^{1/4} t^{1/4} \tag{5.1}$$

for $t \ll t_c$. In a dimensionless form, we write $R_b/a \sim (t/\tau_b)^{1/4}$, where the characteristic time for a bulk to spread by a is $\tau_b = \mu a/\gamma$. Our scaling shows that the radius of the bottom of the bulk increases like $t^{1/4}$, and the rate increases with the initial drop volume and the surface tension while decreasing with the viscosity. Figure 7(*a*) plots the measured data of R_b with time according to the scaling law (5.1) for both water and silicone oil showing that the experiments indeed follow our theory.

The radius of the entire drop footprint $R_t = R_b + L$. As quantitatively validated by figure 2(*d*), the bulk occupies most of the footprint in the early stages of spreading. Such a time range can be deduced by the condition $R_b \gg L$ that leads to $t \ll t_i$, where $t_i \sim a^3\mu r^2/[\gamma h^2(r-1)^2]$ owing to the scalings (4.1) and (5.1). We find that $t_i \sim 1$ and 10 s for water and silicone oil, respectively, for currently tested size ranges of drops. Then we anticipate that R_t will follow the same scaling law as R_b; thus we write

$$R_t \sim \left(\frac{\gamma a^3}{\mu}\right)^{1/4} t^{1/4} \tag{5.2}$$

for $t \ll t_i$. Figure 7(*b*) shows that the experimentally measured radius of the entire footprint follows our scaling law. A linear regression analysis finds the proportionality constant in (5.1) and (5.2) to be 0.438 and 0.552, respectively. In the late stages where L becomes comparable to R_b, the interaction between the collapsing bulk and the wicking flow that originates from the bulk should be taken into account, which calls for further study.

6. Conclusions

We have experimentally investigated the spreading of a liquid drop on superhydrophilic micropillar arrays to find distinctive dynamics of the bulk and the fringe within a single drop. Theoretical models to predict their spreading rates were constructed, which yielded power laws that are in good agreement with experiments. We conclude by discussing our results and their implications. We first showed that

the film flow into a micropillar array arises through the zipping of rows of pillars as a liquid emerges from a micropipette conformally touching the substrate to eliminate the effect of bulk. On the other hand, when there is slight leakage from the pipette tip or a drop is deposited on the substrate, the collapsing portion of the drop, i.e. bulk, pushes a fringe film at a rate $\dot{R}_b$ and leads to circular film spreading. Although the two film propagation modes are seemingly different (faceted versus circular), they share the same dynamical ingredients, i.e. viscous forces resist the wicking force at the periphery of the film. When the front propagation is driven by localized wetting of individual pillars, zipping in the lateral direction could be shown to be energetically more favourable than directly advancing to the next row. However, when the contact line can advance in a way that multiple (s) pillars in the next row can be wet simultaneously, the magnitude of the energy change $\delta E_a = 2h[w(1-2s)+d] < 0$, can be greater than $|\delta E_z|$, or $\delta E_a < \delta E_z$ for $s > (d/w+3)/2$. Such an avalanche-like behaviour may be closely related to the radially outward advancing of the contact line, associated with axisymmetric spreading, when coupled to a bulk. More study is required to elucidate the criteria to determine whether the contact line will zip laterally or advance radially outwards. Considering the capillary forces exerted on a collapsing bulk and the viscous resistance to the flow that effectively slips upon the underlying layer enabled us to estimate the rate of the bulk spreading, which can be applied to the prediction of the entire drop footprint radius in the early stages. Comparing the time scales of the bulk spreading and the fringe extension also indicates that the bulk spreading dominates the initial stages: $\tau_b/\tau_L = (1-1/r)h/a \ll 1$.

Our scaling laws can be a starting point to completely understand the spreading of liquids on superhydrophilic microscopically rough surfaces, which is intrinsically a multi-scale phenomenon, over an entire time range. It will require detailed fluid flow computations considering both the macroscopic radial extension and the microscopic wetting of individual pillars. Our results can be exploited in the analysis of heat and mass transfer of thin spreading films over highly wettable surfaces, whose applications include evaporative cooling (Maclaine-cross & Banks 1984) and absorption refrigeration systems (Teng, Wang & Wu 1997). Also such applications as paper-based microfluidics (Martinez, Phillips & Whitesides 2008) using liquid drops that spread into porous paper can benefit from our analysis.

This work was supported by the National Research Foundation (grants 2009-0067974 and 412-J03001) and KIST, and administered via SNU-IAMD.

Appendix. Shear stress on microdecorated surfaces

Here we estimate the shear stress exerted on a liquid wicking through a micropillar array. The friction occurs due to the basal area, the pillar side walls and the top surface of the pillars. In a unit cell of the micropillar array defined by the area, $(w+d)\times(w+d)$, the viscous shear stress due to the basal area, σ_b, is scaled as $\sigma_b \sim \mu \dot{L}/h_f$, where $\dot{L}$ is the characteristic spreading velocity and h_f is the liquid film thickness measured from the bottom of the surface. The stress due to the side walls of the pillars $\sigma_s \sim \mu \dot{L}/d$. The pressure drop of the flow passing around a pillar is $\Delta p \sim \mu \dot{L}/h$, where we used the fact that $h_f \approx h \approx d$ in our experiments. This pressure drop should hold for the flow on the pillar tops leading to $\dot{L}/h \sim u_t/h_t$, where u_t and $h_t = h_f - h$ are the flow speed and the thickness of the liquid film on the pillar tops, respectively. We find $u_t/\dot{L} \ll 1$ because $h_t \ll h$, which corresponds to the experimental observation. Then the stress due to the top of the pillars scales as $\sigma_t \sim \mu \dot{L}/h$. Taking

the total shear stress σ as a weighted average of those stresses, $\sigma = \phi_b\sigma_b + \phi_t\sigma_t + \phi_s\sigma_s$, where ϕ_b, ϕ_t, ϕ_s is the area fraction of the base and the top and the sides of a pillar, respectively, we get

$$\sigma \sim \frac{\mu r \dot{L}}{h}. \tag{A 1}$$

REFERENCES

Biance, A.-L., Clanet, C. & Quéré, D. 2004 First steps in the spreading of a liquid droplet. *Phys. Rev.* E **69**, 016301.

Brochard-Wyart, F., Debrégeas, G. & de Gennes, P. G. 1996 Spreading of viscous droplets on a non viscous liquid. *Colloid Polym. Sci.* **274**, 70–72.

Cassie, A. B. D. & Baxter, S. 1944 Wettability of porous surfaces. *Trans. Faraday Soc.* **40**, 546–551.

Courbin, L., Denieul, E., Dressaire, E., Roper, M., Ajdari, A. & Stone, H. A. 2007 Imbibition by polygonal spreading on microdecorated surfaces. *Nature Mater.* **6**, 660–664.

de Gennes, P. G. 1985 Wetting: statics and dynamics. *Rev. Mod. Phys.* **57**, 827–863.

Ehrhard, P. 1993 Experiments on isothermal and non-isothermal spreading. *J. Fluid Mech.* **257**, 463–483.

Huppert, H. E. 1982 The propagation of two-dimensional and axisymmetric viscous gravity currents over a rigid horizontal surface. *J. Fluid Mech.* **121**, 43–58.

Ishino, C., Reyssat, M., Reyssat, E., Okumura, K. & Quéré, D. 2007 Wicking within forests of micropillars. *Europhys. Lett.* **79**, 56005.

Lopez, J. & Miller, C. A. 1976 Spreading kinetics of liquid drops on solids. *J. Colloid Interface Sci.* **56** (3), 460–468.

Maclaine-cross, I. L. & Banks, P. J. 1981 A general theory of wet surface heat exchangers and its application to regenerative evaporative cooling. *Trans. ASME J. Heat Transfer* **103**, 579–585.

Martinez, A. W., Phillips, S. T. & Whitesides, G. M. 2008 Three-dimensional microfluidic devices fabricated in layered paper and tape. *Proc. Natl Acad. Sci. USA* **105**, 19606–19611.

McHale, G., Shirtcliffe, N. J., Aqil, S., Perry, C. C. & Newton, M. I. 2004 Topography driven spreading. *Phys. Rev. Lett.* **93**, 036102.

Reyssat, M., Courbin, L., Reyssat, E. & Stone, H. A. 2008 Imbibition in geometries with axial variations. *J. Fluid Mech.* **615**, 335–344.

Sbragaglia, M., Peters, A. M., Pirat, C., Borkent, B. M., Lammertink, R. G. H., Wessling, M. & Lohse, D. 2007 Spontaneous breakdown of superhydrophobicity. *Phys. Rev. Lett.* **99**, 156001.

Tanner, L. H. 1979 The spreading of silicone oil drops on horizontal surfaces. *J. Phys. D: Appl. Phys.* **12**, 1473–1484.

Teng, Y., Wang, R. Z. & Wu, J. Y. 1997 Study of the fundamentals of adsorption systems. *Appl. Therm. Engng* **17**, 327–338.

Washburn, E. W. 1921 The dynamics of capillary flow. *Phys. Rev.* **17**, 273–283.

Wenzel, R. N. 1936 Resistance of solid surfaces to wetting by water. *Ind. Engng Chem.* **28**, 988–994.

Yi, J. W., Moon, M.-W., Ahmed, S. F., Kim, H., Cha, T.-G., Kim, H.-Y., Kim, S.-S. & Lee, K.-R. 2010 Long-lasting hydrophilicity on nanostructured Si-incorporated diamond-like carbon films. *Langmuir* **26**, 17203–17209.